AIAA JOURNAL
Vol. 43, No. 12, December 2005

Near-Field Measurements in an Equilateral Triangular Turbulent Freejet

W. R. Quinn*
St. Francis Xavier University, Antigonish, Nova Scotia B2G 2W5, Canada

The near-field mean flow and turbulence characteristics of a turbulent jet of air issuing from a sharp-edged equilateral triangular orifice into still air surroundings have been examined experimentally using hot-wire anemometry and a pitot-static tube. For comparison, some measurements were made in a round free air jet, also issuing from sharp-edged orifice. The Reynolds number, based on the equivalent diameter, was 1.84×10^5 in each jet. The three components of the mean velocity vector, the Reynolds normal and primary shear stresses, the distribution of the autocorrelation coefficients and the one-dimensional energy spectra of the fluctuating velocity signals, and the mean static pressure were measured. The mean streamwise vorticity, the half-velocity widths, mass entrainment into the jet, and the local shear in the mean streamwise velocity were obtained from the measured data. It was found that mixing in the equilateral triangular jet is faster than in the round jet. The mean streamwise vorticity field was found to be dominated by counter-rotating pairs of vortices, which facilitated mixing and entrainment in the equilateral triangular jet. The distribution of the autocorrelation coefficients and the one-dimensional energy spectra results indicated the presence of coherent structures in the near field of the equilateral triangular jet.

Nomenclature

A, C	=	constants in the hot-wire exponent power law
B	=	jet half-velocity width
D	=	diameter
E	=	hot-wire output voltage
f	=	frequency
k	=	turbulence kinetic energy
n	=	exponent in the hot-wire exponent power law
P	=	mean static pressure
Q	=	mass flow rate at a streamwise location
t	=	time
U	=	streamwise component of the mean velocity vector
$\overline{u'^2}$	=	streamwise Reynolds normal stress
$\sqrt{\overline{u'^2}}$	=	root-mean-square of the streamwise fluctuating velocity
$\overline{u'v'}$	=	spanwise Reynolds primary shear stress
$\overline{u'w'}$	=	lateral Reynolds primary shear stress
V	=	spanwise component of the mean velocity vector
$\overline{v'^2}$	=	spanwise Reynolds normal stress
$\sqrt{\overline{v'^2}}$	=	root-mean-square of the spanwise fluctuating velocity
W	=	lateral component of the mean velocity vector
$\overline{w'^2}$	=	lateral Reynolds normal stress
$\sqrt{\overline{w'^2}}$	=	root-mean-square of the lateral fluctuating velocity
X	=	streamwise coordinate
Y	=	spanwise coordinate
Z	=	lateral coordinate
ε	=	dissipation of turbulence kinetic energy
ν_t	=	turbulent (or eddy) kinematic viscosity
ρ	=	density of the jet fluid
$\rho(\tau)$	=	correlation coefficient
σ	=	generic fluctuating velocity
Φ	=	power spectral density
Ω	=	mean streamwise vorticity

Subscripts

atm	=	atmospheric value of P
cl	=	value of U anywhere on the jet centerline
e	=	equivalent value of D for a noncircular orifice or geometric mean value of B
eff	=	effective hot-wire cooling velocity
exit	=	value of U at the center of the orifice exit plane
max	=	maximum value of U on the jet centerline
o	=	value of Q at the orifice exit plane
s	=	static value of P
x	=	streamwise value of Ω
$\frac{1}{2}$	=	half-velocity width value

Introduction

JETS are important parts of many processes in engineering. The study of jets is, therefore, relevant not only from the fundamental viewpoint but also because of technical applications. Jets issuing from noncircular orifices with corners, such as square, rectangular, or triangular, are especially important in combustion systems in which large-scale mixing, initiated at the flat sides of the orifice, and small-scale mixing, in the corner regions, are required. The combustion process needs large-scale mixing to promote bulk mixing of the fuel and oxidizer and small-scale mixing to facilitate chemical reactions. Expedient manufacturing and installation ease will dictate that a noncircular orifice, such as a triangular orifice, be made by machining flat work pieces, with resulting sharp edges, which are then appropriately assembled to obtain the orifice shape. A sharp-edged triangular orifice is, therefore, used in the current study. In practical systems, corner radii will have to be included to inhibit the initiation and propagation of cracks. Experiments on triangular and other noncircular orifices with corner radii are currently underway in our laboratory.

Studies of noncircular jets in the extant archival literature up to 1997 have been reviewed by Gutmark and Grinstein.[1] Only the studies of Vandsburger and Ding[2] and Quinn[3] are entirely devoted to the turbulent jet issuing from an equilateral triangular orifice. In the study of Vandsburger and Ding,[2] active control of the jet, introduced at the exit plane through azimuthal axisymmetric and helical modes of excitation, was used to examine the evolution of the jet up to 30 hydraulic diameters downstream from the orifice exit plane. Quinn[3] presented experimental data for the three components of the mean velocity vector, the three turbulent normal stresses, and the two turbulent primary shear stresses. Shadow et al.[4] examined equilateral

Received 3 November 2004; revision received 5 April 2005; accepted for publication 10 May 2005.

*Professor, Department of Engineering; wquinn@stfx.ca. Senior Member AIAA.

and isosceles triangular jets issuing on the one hand from pipes and on the other hand from orifices. In the case of equilateral triangular jets, it was found that, whereas the momentum thickness of the shear layer at the vertex side was 35% larger than that at the flat side, spreading at the center of the flat side was greater than that at the vertex and this resulted in the jet acquiring a quasi-circular shape at $X/D_e = 5.0$. Distinct peaks were found in the spectral distribution of the flow energy at the flat sides compared to a broadband distribution at the vertices. Gutmark et al.[5] found that flames issuing from equilateral triangular burners had the cross-sectional shape of the burner exit plane in the very near field, $X/D_e = 0.3$. The shape of the flame cross section then became quasi circular at $X/D_e = 1.9$ and at $X/D_e = 2.5$, and farther downstream, at $X/D_e = 3.1$, the flame shape became triangular again but inverted compared to the triangular shape at the exit. They also found, in agreement with their earlier cold-flow measurements, large-scale vortices at the flat sides of the burner and an unstructured flame at the vertex. Miller et al.[6] performed a numerical study, using direct numerical simulation, of jets issuing from circular, elliptic, square, rectangular, and equilateral triangular and isosceles triangular nozzles into coflowing surroundings at a Reynolds number, based on the nozzle equivalent diameter and the velocity difference between the jet and the coflowing stream, of 8×10^2. The aspect ratio of the elliptic and rectangular nozzles was 2:1. The isosceles triangular jet, in terms of mixing enhancement relative to the circular jet, was found to be the most efficient. The mean streamwise velocity decay on the jet centerline, mass entrainment, and product formation amount, in the case of reacting jets, were used as measures to arrive at the conclusion made in the study. Mi et al.[7] studied experimentally the mean streamwise velocity decay and streamwise turbulence intensity behavior along the jet centerline for the circular and a number of noncircular turbulent freejets at a Reynolds number, based on orifice equivalent diameter, of 1.5×10^4. The study concluded that the jet from the isosceles triangular orifice had the best mixing enhancement characteristics relative to the circular jet.

The present study was undertaken to extend the scope of the work reported by Quinn.[3] The objective is to contribute to the processes of mixing and entrainment in the jet and to provide detailed mean flow and turbulence data that can be used to facilitate the numerical computation of the flow. Mass entrainment and the mean streamwise vorticity, which have been obtained from the mean flow data, and mean static pressure data are also presented, along with the distribution of the autocorrelation coefficients and the one-dimensional energy spectra of the fluctuating streamwise velocity signals.

Flow Facility

The jet flow facility used for the present study is shown in Fig. 1. It consists of a small centrifugal fan, a diffuser, a settling chamber, a three-dimensional contraction, and a screen cage. The fan, which drew air from a room adjacent to the laboratory and delivered it to the equilateral triangular orifice via the diffuser, settling chamber, and contraction, was supported on antivibration neoprene pads. The diffuser was fitted with a baffle at its upstream end, honeycomb, and mesh-wire screens. The settling chamber, a plywood box of 0.762×0.762 m cross section and 1.054-m length, was also fitted with mesh-wire screens. The three-dimensional contraction had a contour that is a third-degree polynomial that had zero derivatives as end conditions. The contraction, 0.523 m in length, had a circular cross section, with 0.762-m diameter at its upstream end and a 0.305×0.305 m square cross section at its downstream end. The equilateral triangular orifice, shown in Fig. 2, capped the downstream end of the contraction, which was flush with a 2.438×2.438 m plywood wall. The coordinate system used is shown in Fig. 2. The streamwise X coordinate, which is not shown, is perpendicular to the spanwise Y and lateral Z coordinates and forms a right-hand system with them. The flow, as viewed from section A–A in Fig. 2, is from left to right. The contraction ratio was 283. The plywood wall formed one side of a screen cage which extended 3.658 m downstream from the wall. The experiments were performed in a $7.70 \times 7.01 \times 2.87$ m room.

A three-dimensional traversing system was used for moving the sensing probes in the flowfield. The system consisted of a rack and pinion for traversing in the X direction and lead screws for traversing in the Y and Z directions. The base of the traversing

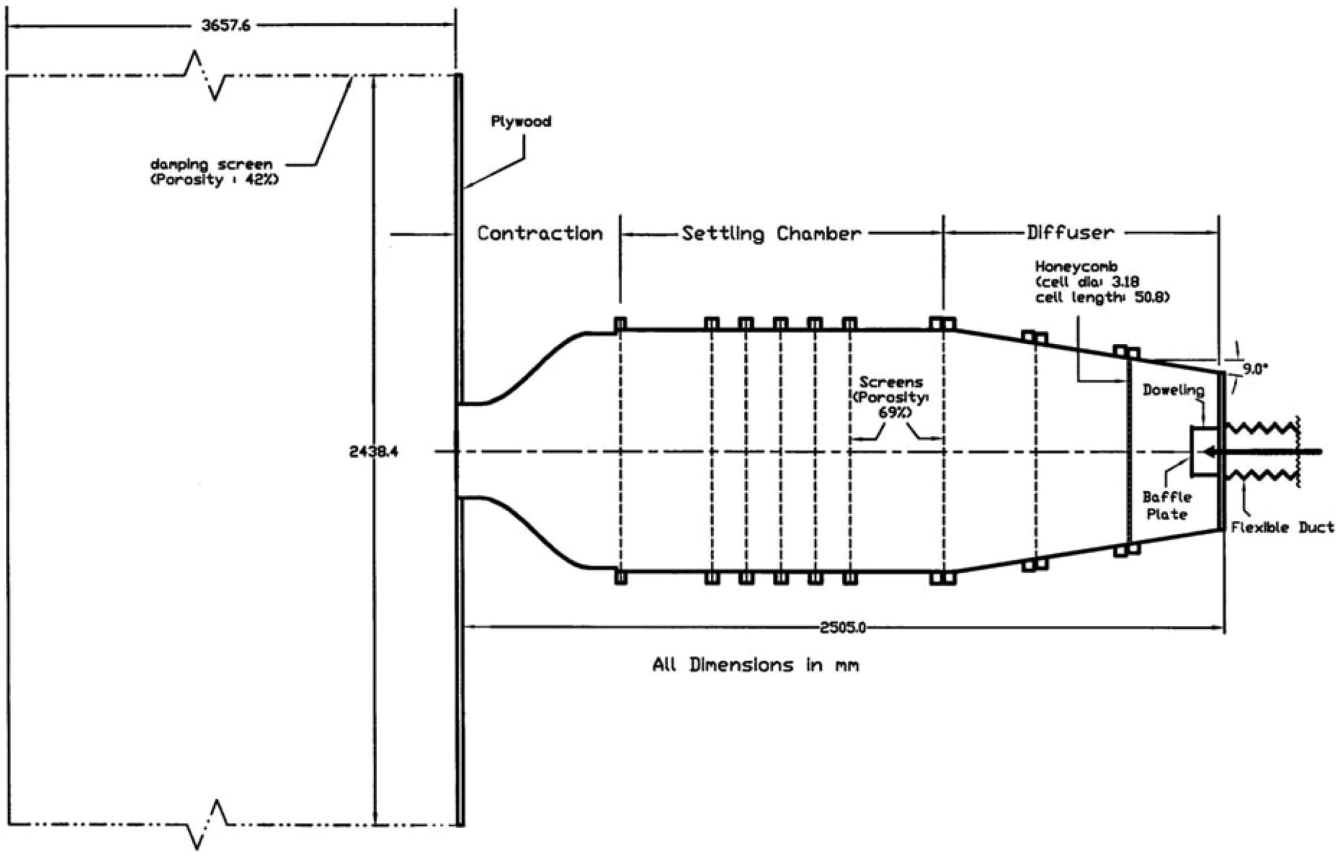

Fig. 1 Plan view section of flow facility.

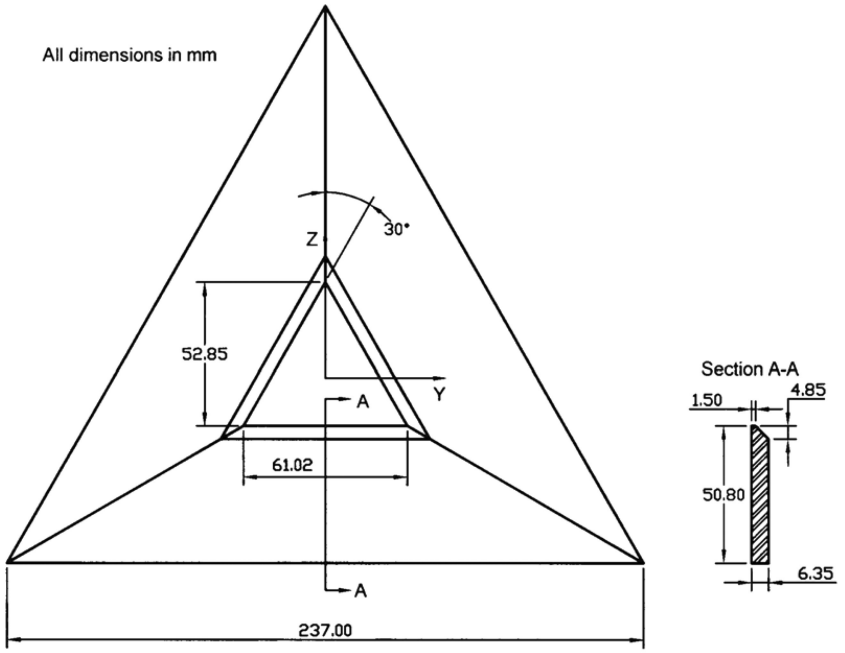

Fig. 2 Equilateral triangular orifice.

system was, like the fan, also supported on antivibration neoprene pads. Traversing in all three coordinate directions was effected by microcomputer-controlled stepping motors. Positioning accuracy of the sensing probes was 0.3 mm in the X direction and 0.01 mm in both the Y and Z directions. The data were acquired on a grid, in the Y–Z plane, at each X location. The grid spacing, which was kept the same in the Y and Z directions, varied from 2.54 mm close to the jet exit to 12.7 mm farther downstream.

Flow Diagnostic Tools

The mean velocity and turbulence data were acquired with DANTEC P51 X-array probes. These probes consist of two 5-μm-diam platinum-plated tungsten slant wire sensing elements about 1 mm long and about 1 mm apart. The hot-wire probes, operated by DANTEC constant temperature anemometers at a resistance ratio of 1.8, were calibrated online close to the exit of the jet against the output of a pitot-static tube, which was connected to a pressure transducer and a Barocel electronic manometer. The calibration data were fitted to the exponent power law: $E^2 = A + CU_{\text{eff}}^n$ and A, C, and n were optimized with a linear least-squares goodness-of-fit procedure. A cosine law response to yaw was assumed, and the effective angle was found from a yaw calibration following the procedure described by Bradshaw.[8] Temperature variations from the calibration temperature were monitored with a thermocouple placed in proximity to the hot-wire probe, and corrections for such variations were made using the procedure by Bearman[9] in the data-reduction software. The mean flow and turbulence data were corrected for the effect of the mean velocity gradients on the spacing between the two slant sensing-wire elements of the X-array probes by using the formulas given by Bell and Mehta.[10]

The hot-wire signals were linearized by the laboratory microcomputer and digitized, along with the signals from the thermocouple, with the National Instruments AT-A2150 dynamic signal acquisition board. This board consists of four analog input channels, each of 16-bit resolution. Each of the analog input channels is preceded by a third-order Butterworth low-pass analog antialiasing filter with an 80-kHz cutoff. The filtered signal is sampled with a 1-bit delta–sigma modulating analog sampler at 64 times the chosen sampling rate. This reduces the quantization noise considerably. The output of the sampler is then fed to a digital antialiasing filter, which is built into the A/D converter chip, and the output of this filter resamples the signal to the data rate, namely, 16-bit digital samples. Note that all four analog input channels can be sampled simultaneously and, therefore, no sample-and-hold units, which are required for successive approximation and dual slope A/D converters, are needed here. The input range of the AT-A2150 board is ± 2.828 V (or 2 V rms) so that amplification was only needed for the thermocouple signal and not for the hot-wire signals. The mean velocity and turbulence data were obtained from records containing 8192 samples acquired at a sampling rate of 4 kHz.

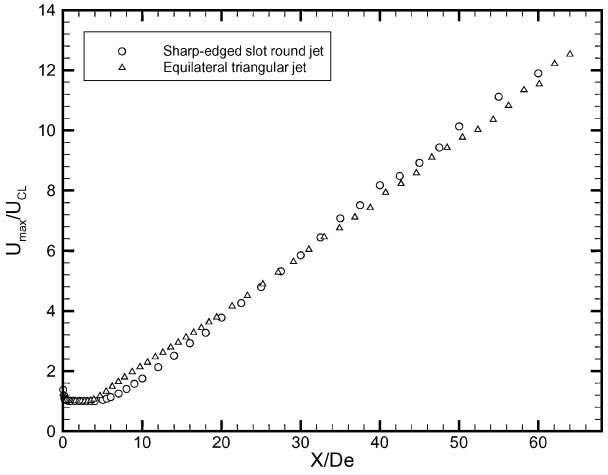

Fig. 3 Mean streamwise velocity decay on jet centerline.

The mean static pressure measurements were made with 2.3-mm-diam pitot-static tube, made of stainless steel with an ellipsoidal head and four circumferentially located static pressure holes. It was connected to a DATAMETRICS pressure transducer and an electronic manometer. These signals were also digitized with the AT-A2150 board, but a voltage divider was needed to bring the signals into the input range of the board.

Initial Conditions

The mean streamwise velocity at the center of the orifice exit plane was 61 m/s, and this resulted in a Reynolds number, based on the orifice equivalent diameter $D_e = 45.3$ mm, of 1.84×10^5. The streamwise turbulence intensity at the orifice exit plane was 0.4%.

Results and Discussion

The decay of the mean streamwise velocity along the centerline of the jet is shown in Fig. 3. The data, acquired in our laboratory,

for a round jet issuing from a sharp-edged orifice are included for comparison. Note that the diameter of the sharp-edged round orifice is the same as the equivalent diameter of the equilateral triangular orifice and that both of the orifices had the same exit area. The data for both the equilateral triangular and round jets in the present study were obtained at the same Reynolds number of 1.84×10^5. The $U_{\max}/U_{\mathrm{cl}}$ value at the exit plane is greater than unity in both jets due to the vena contracta effect, which is associated with sharp-edged orifices. Note that both $U_{\max}$ and U_{cl} are actual values of the mean streamwise velocity on the jet centerline. The potential core lengths of the equilateral triangular and round jets are $2.71D_e$ and $3.50\ D_e$, respectively, and this implies faster mixing in the equilateral triangular jet compared to that in the round jet. Figure 3 also shows that the decay of the equilateral triangular jet is steeper than that of the round jet up to about $X/D_e = 20$, again indicating enhanced mixing in the equilateral triangular jet compared that in the round jet in this region of the flow. The estimated uncertainty in the measurement of the mean streamwise velocity is $\pm 1\%$ at 20:1 odds. The odds in all uncertainties given subsequently will be the same, that is, 20:1, and will, therefore, not be restated.

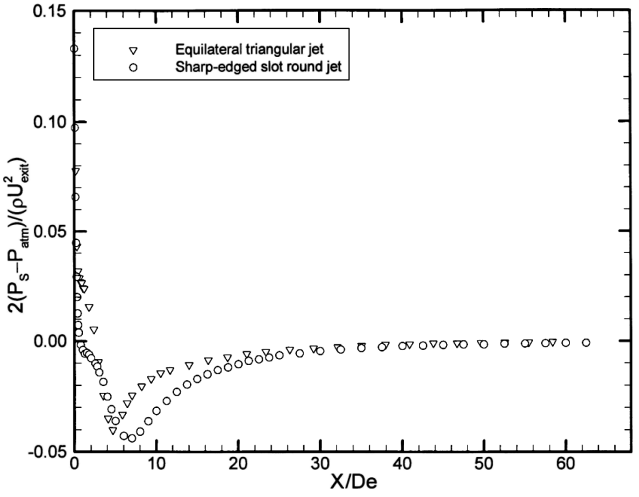

Fig. 4 Mean static pressure variation on jet centerline.

The mean static pressure distribution on the jet centerline for the equilateral triangular jet is shown in Fig. 4. The data for the round jet are also shown for comparison. Both jets exhibit similar behavior in the very near flowfield, namely, the mean static pressure drops from a positive value, that is, above atmospheric pressure, at the slot exit plane to zero, that is, atmospheric pressure, as a result of the acceleration of the jet fluid brought about by the vena contracta effect. The further decrease in the mean static pressure to negative values is triggered by the rapid production of turbulence from mean flow shear in the near flowfield. The speed with which the mean static pressure in a jet recovers from negative values to atmospheric pressure can, perhaps, be taken as a measure of how fast mixing is taking place within the jet. Based on this, mixing in the equilateral triangular jet is faster than that in the round jet. The uncertainty in the measurement of the mean static pressure is $\pm 1\%$.

The contour maps for the mean streamwise velocity are shown in Fig. 5. Note that the contour plots in Fig. 5 and those shown subsequently are only for a small subset of the streamwise locations shown in Fig. 3. Initially, at $X/D_e = 0.5$, the contours have the equilateral triangular shape of the orifice and they are very closely spaced, indicating that very little mixing has taken place at this location. At $X/D_e = 1.0$, the contours have acquired a quasi-circular shape and the spacing between the contour levels has increased. Farther downstream, at $X/D_e = 2.0$, the contours have the inverted shape of the equilateral triangle at the orifice exit plane; this has been referred to as axis switching by various investigators of noncircular jets. The spacing between the contour levels has increased farther at

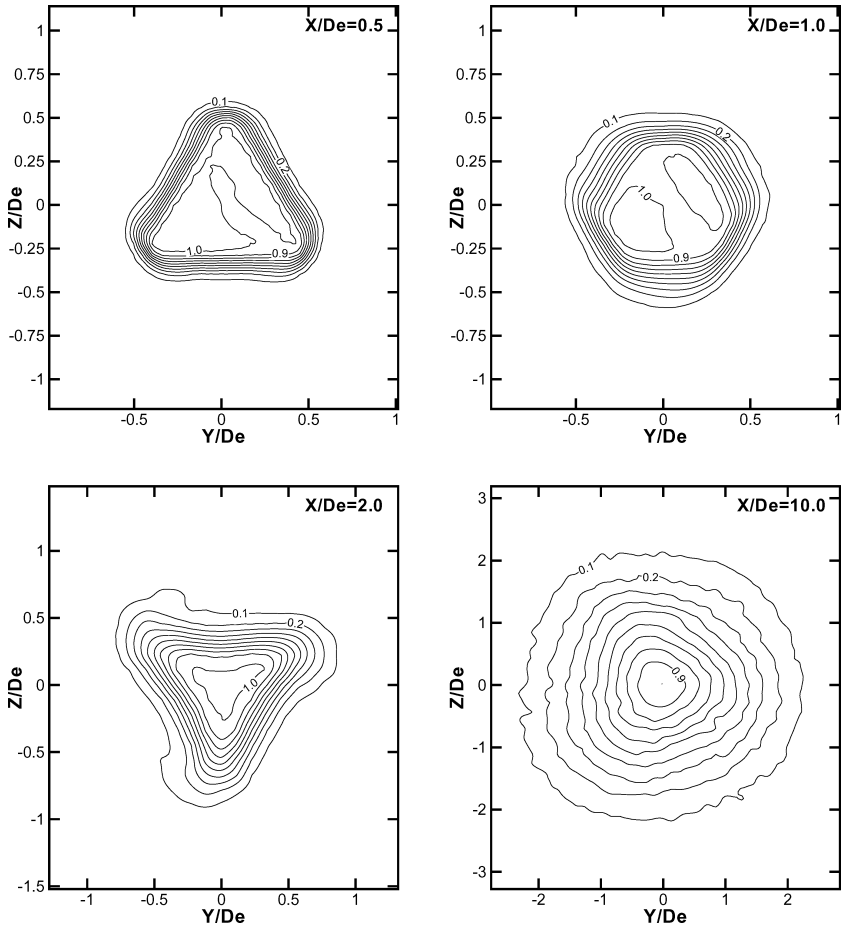

Fig. 5 Mean streamwise velocity, U/U_{cl}, contour maps.

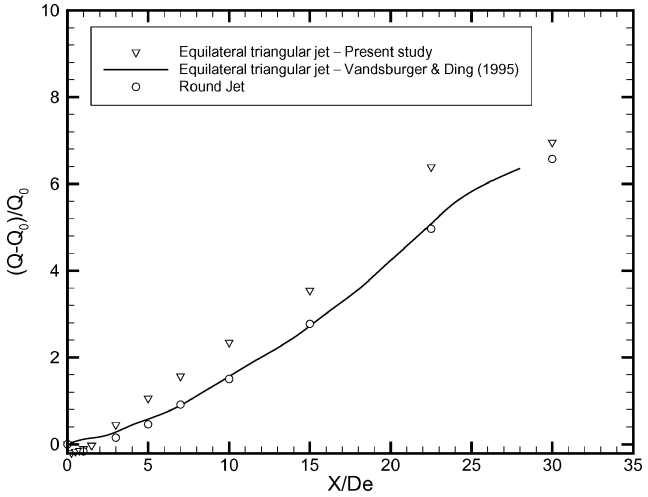

Fig. 6 Mass entrainment into jet.

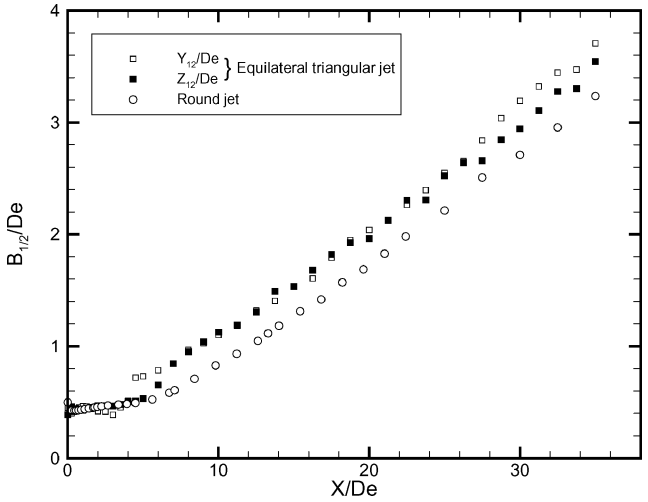

Fig. 7 Development of jet half-velocity widths.

this location, implying that mixing is taking place. Some memory of the initial equilateral triangular shape is still evident in the inner part of the contour map at $X/D_e = 10.0$, even though the outer contours are more or less circular. The observations of the mean streamwise velocity field at $X/D_e = 0.5$, 1.0, and 10.0 in the present study are in agreement with those made by Quinn[3] for a jet issuing from a sharp-edged equilateral triangular orifice.

Mass entrainment into the jet has been calculated from the mean streamwise velocity data by numerical quadrature, and the results are shown in Fig. 6 for the equilateral triangular and round jets. The data for the unforced equilateral triangular jet in the study of Vandsburger and Ding[2] are included for comparison. The equilateral triangular jet clearly has a larger mass entrainment than the round jet up to $X/D_e = 30$, again implying a faster rate of mixing in the equilateral triangular jet compared to that in the round jet. The mass entrainment data for the unforced equilateral triangular jet studied by Vandsburger and Ding[2] are more or less the same as those of the round jet of the present study. Note that the flow Reynolds number and the exit plane turbulence intensity in the jet in Vandsburger and Ding[2] were 8×10^3 and 1%, respectively, compared to 1.84×10^5 and 0.4%, respectively, in the jets of this study. The evolution of jets is known to depend on initial conditions.

The development of the jet half-velocity widths in the X–Y and X–Z planes, taken through the origin of the coordinate system in Fig. 2, is shown in Fig. 7 for the equilateral and round jets studied here. The half-velocity width of a jet is defined as the distance from the centerline of the jet to the point where the mean streamwise velocity is half its value on the jet centerline. The half-velocity widths

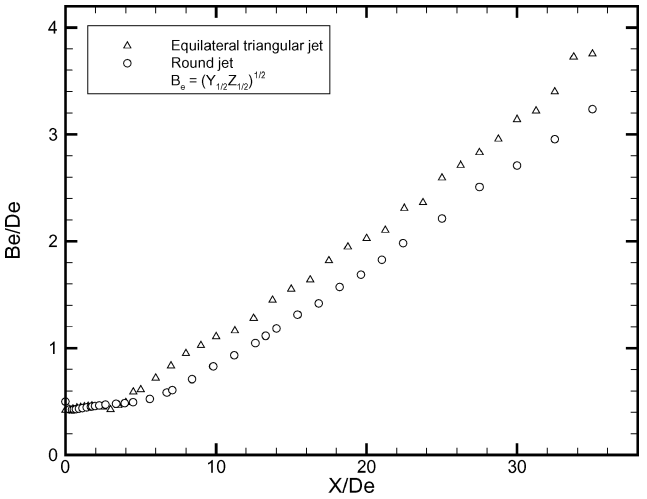

Fig. 8 Geometric mean of jet half-velocity widths.

of the equilateral triangular jet in both the X–Y and X–Z planes decrease initially, due to the vena contracta effect, and then increase monotonically with downstream distance triggered by the large-scale structures emanating from all three flat sides. Axis switching, a phenomenon observed by others who have studied noncircular jets, takes place several times, not surprisingly given the symmetry of the jet. The half-velocity widths of the equilateral triangular jet are clearly larger than the round jet half-velocity widths at all of the streamwise locations considered in the present study. This again points to faster mixing in the equilateral triangular jet compared to that in the round jet.

The geometric mean of the half-velocity widths, $B_e = (Y_{1/2}Z_{1/2})^{0.5}$, is used to facilitate a clear comparison of the spread of the two jets of the present study. The data are shown in Fig. 8, from which it is clear, as has already been indicated by the mean static pressure data on the jet centerline shown in Fig. 4 and the mass entrainment data shown in Fig. 6, that the equilateral triangular jet spreads faster than the round jet.

The mean static pressure contour maps are shown in Fig. 9. The mean static pressure distribution along the jet centerline presented in Fig. 4 showed positive values up to about $X/D_e = 3$ and negative values up to about $X/D_e = 20$. It is, therefore, not surprising to find positive mean static pressures in the central regions of the jet at $X/D_e = 0.25$, 1.0, and 2.0 and negative mean static pressures throughout the jet at $X/D_e = 10.0$ in Fig. 9. It is clear that ambient fluid will generally be pumped into the jet as result of the difference in pressure between the ambient and the jet. This is the case at $X/D_e = 10.0$. At the other three locations shown in Fig. 9, regions of positive mean static pressure within the jet will pump jet fluid into regions of negative mean static pressure. At $X/D_e = 0.25$, for example, jet fluid will be pumped from the region inside the equilateral triangle into the corners, which will, in turn, receive ambient fluid and, at $X/D_e = 1.0$, fluid will be pumped from the jet potential core into the shear layers that are aligned with the sides of the equilateral triangle.

Mean streamwise vorticity was calculated from the V and W data by applying a central differencing procedure to the formula $\Omega_x = [\partial W/\partial Y - \partial V/\partial Z]$, and the results are shown as contour maps in Fig. 10. The uncertainty in the mean streamwise vorticity data is estimated to be ±19.5%. Remember that, because vorticity cannot be created within the core of a homogeneous fluid, vortices in the unbounded flow considered here must necessarily exist as counter-rotating pairs. Also, positive and negative Ω_x indicate counterclockwise and clockwise rotation, respectively, consistent with the right-hand system used here. The mean streamwise vorticity field of this jet is clearly complex. At $X/D_e = 0.5$, the mean streamwise vorticity field consists of three outflow pairs of counter-rotating vortices, aligned with the corners of the equilateral triangle. The mutual induction of these outflow vortex pairs, as they are referred to in the literature, results in the sideways movement

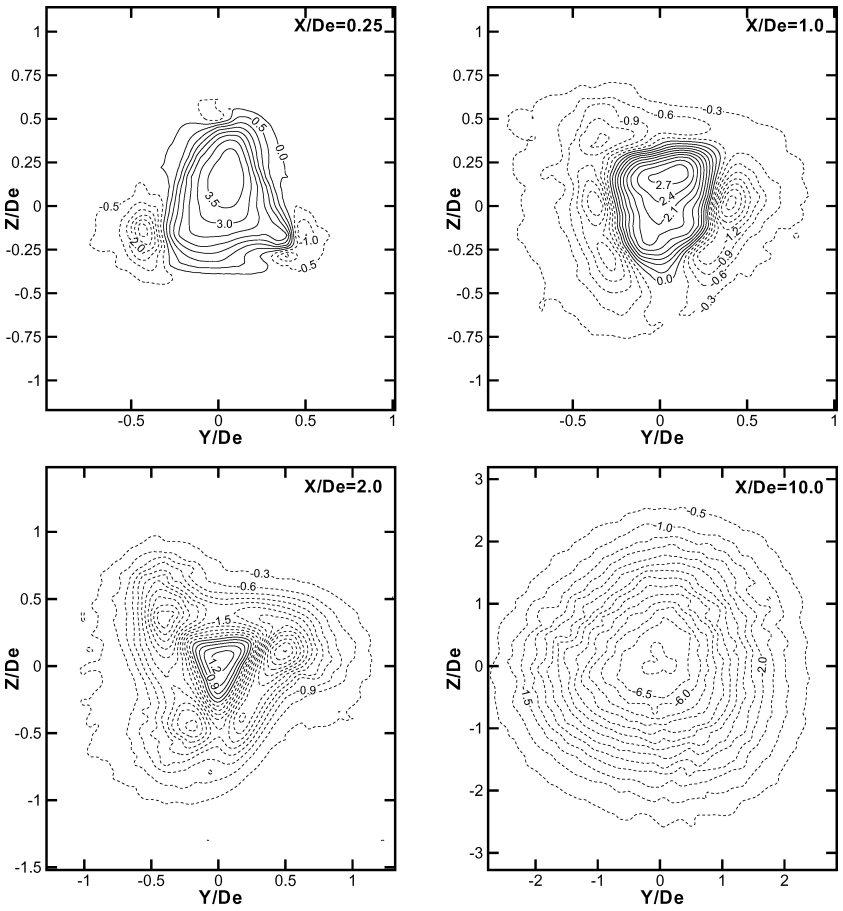

Fig. 9 Mean static pressure, $(2(P_s - P_{\text{atm}})/\rho U_{\text{cl}}^2) \times 100$, contour maps.

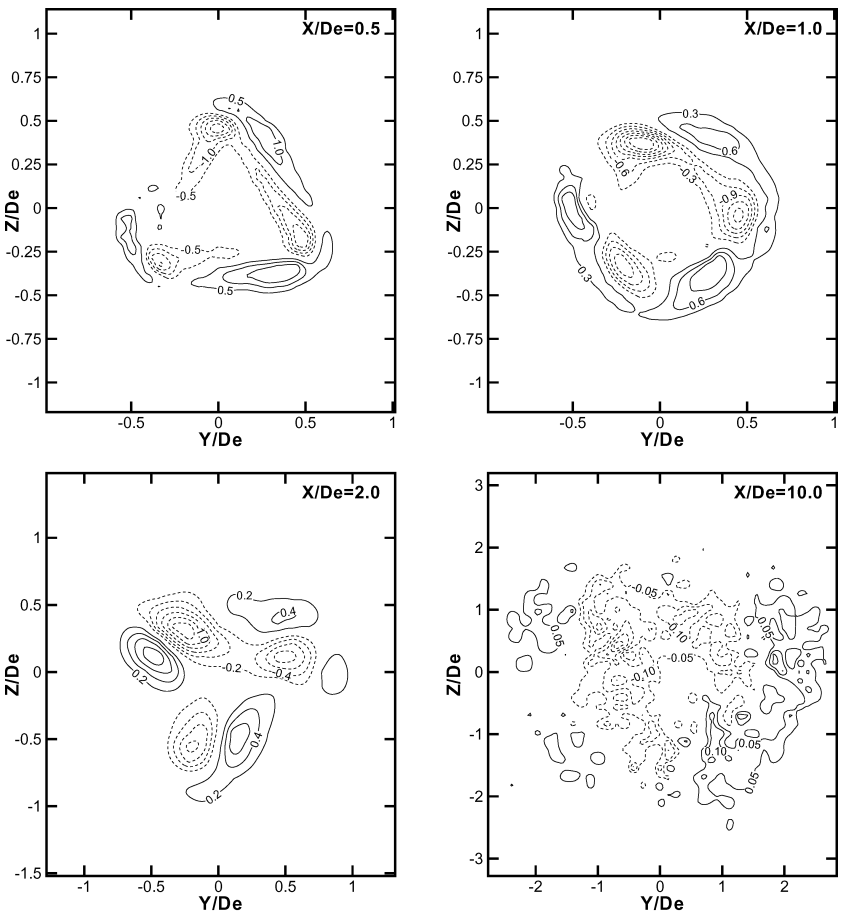

Fig. 10 Mean streamwise vorticity, $\Omega_x D_e/U_{\text{cl}}$, contour maps.

of all of the three sides of the equilateral triangle. The dynamics of these vortex pairs ultimately produces the quasi-circular shape of the mean streamwise velocity contour map $X/D_e = 1.0$ in Fig. 5. At $X/D_e = 1.0$, two pairs of outflow, at the top of the quasi-circular shape prescribed by the mean streamwise velocity contour map at this location, shown in Fig. 5, and two pairs of inflow, at the bottom of the aforementioned quasi-circular shape, counter-rotating vortices can be identified in the mean streamwise vorticity field. The mutual induction of these outflow and inflow vortex pairs causes, respectively, the outward movement of the top and the inward movement of the bottom, of the quasi-circular shape referred to earlier and, thus, leads to the 180-deg rotation of the initial equilateral triangular shape of the mean streamwise velocity contour map at $X/D_e = 2.0$, shown in Fig. 5. This has been referred to as the axis-switching phenomenon in the literature on noncircular jets, as already mentioned. The mean streamwise vorticity contour map at $X/D_e = 2.0$ also consists of three outflow pairs of counter-rotating vortices, now aligned with the corners of the inverted equilateral triangular shape at this location. The mutual induction of these outflow vortex pairs results in motion toward the center of jet, as clearly seen here. This movement of the counter-rotating vortex pairs toward the center of the jet was also observed in the square jet study of Quinn.[11] Viscosity has clearly diffused the vorticity at $X/D_e = 10.0$, as the mean streamwise vorticity contour map at this location shows.

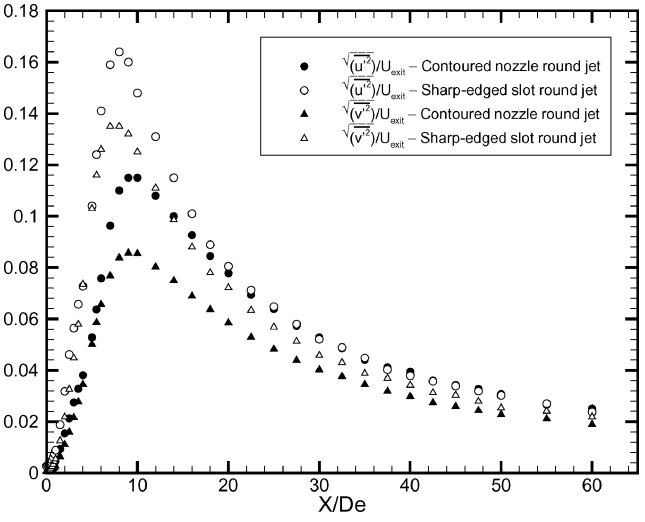

Fig. 11 Evolution of turbulence intensities along jet centerline.

The evolution of the streamwise, $\sqrt{u'^2}/U_{\text{exit}}$, spanwise, $\sqrt{v'^2}/U_{\text{exit}}$, and lateral, $\sqrt{w'^2}/U_{\text{exit}}$, turbulence intensities, along with streamwise turbulence intensity data for a round jet, is shown in Fig. 11. A steep initial increase in all of the turbulence intensities is observed. This is brought about by the production of turbulence from the mean flow shear in the shear layers emanating from all three sides of the equilateral triangle and diffusion of the turbulence from the shear layers to the jet centerline. The turbulence intensities in the equilateral triangular jet peak at $X/D_e = 5.43$ before the streamwise turbulence intensity in the round jet reaches its peak value at $X/D_e = 8.0$, an indication of enhanced mixing in the equilateral triangular jet. Recall that the mean static pressure along the jet centerline in the equilateral triangular jet, shown in Fig. 4, also starts to recover from negative values toward atmospheric pressure at $X/D_e = 4.67$ before the mean static pressure in the round jet does at $X/D_e = 7.0$.

Contour maps for the streamwise, spanwise, and lateral Reynolds normal stresses are shown in Figs. 12–14. The shapes of these contour maps correspond very closely to those of the mean streamwise velocity shown in Fig. 5 at the corresponding streamwise locations. Large or small values of the streamwise, spanwise, or lateral Reynolds normal stress are found, as is to be expected, in regions

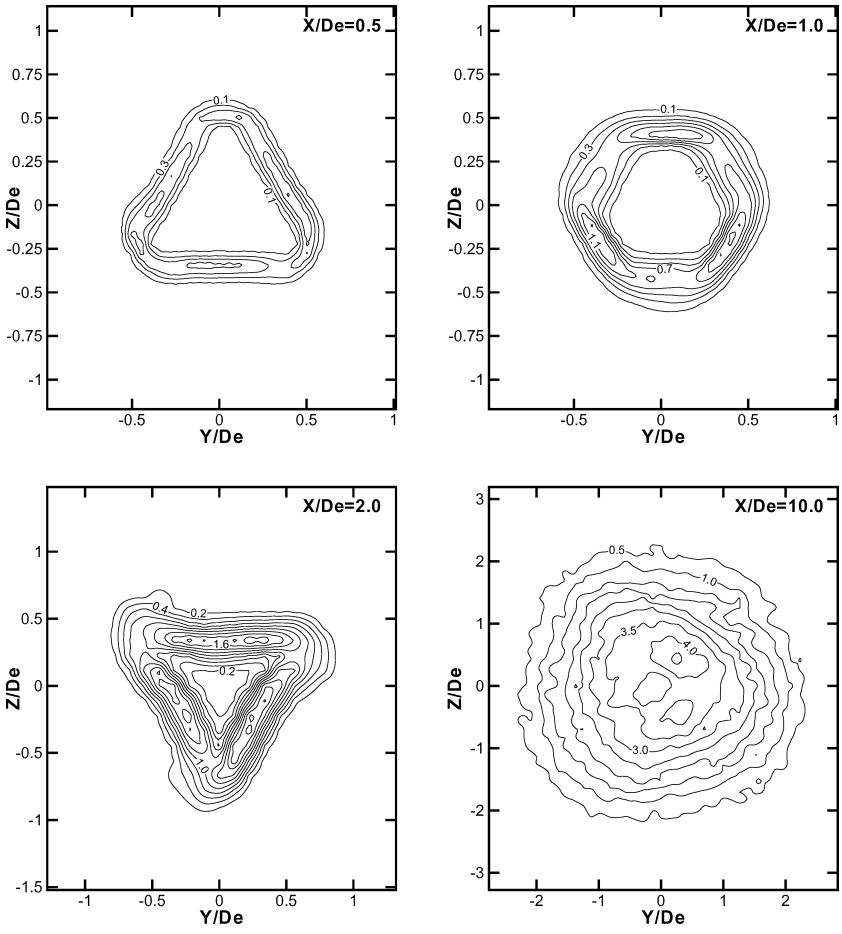

Fig. 12 Streamwise Reynolds normal stress, $\overline{u'^2}/U_{\text{cl}}^2 \times 100$, contour maps.

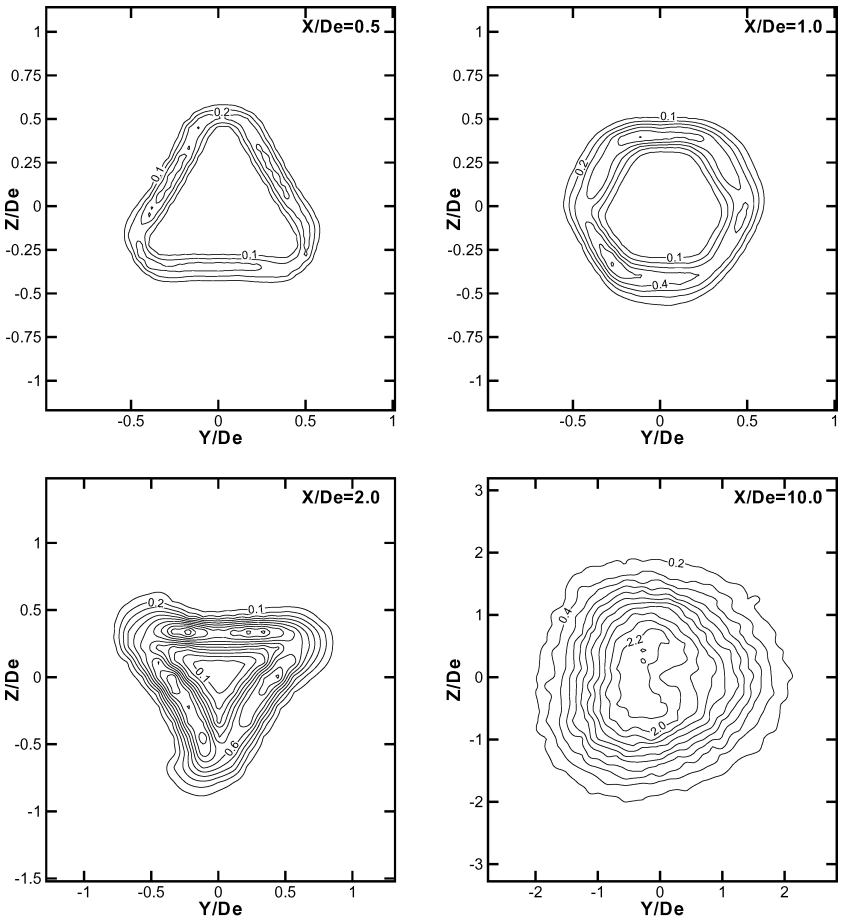

Fig. 13 Spanwise Reynolds normal stress, $\overline{v'^2}/U_{cl}^2 \times 100$, contour maps.

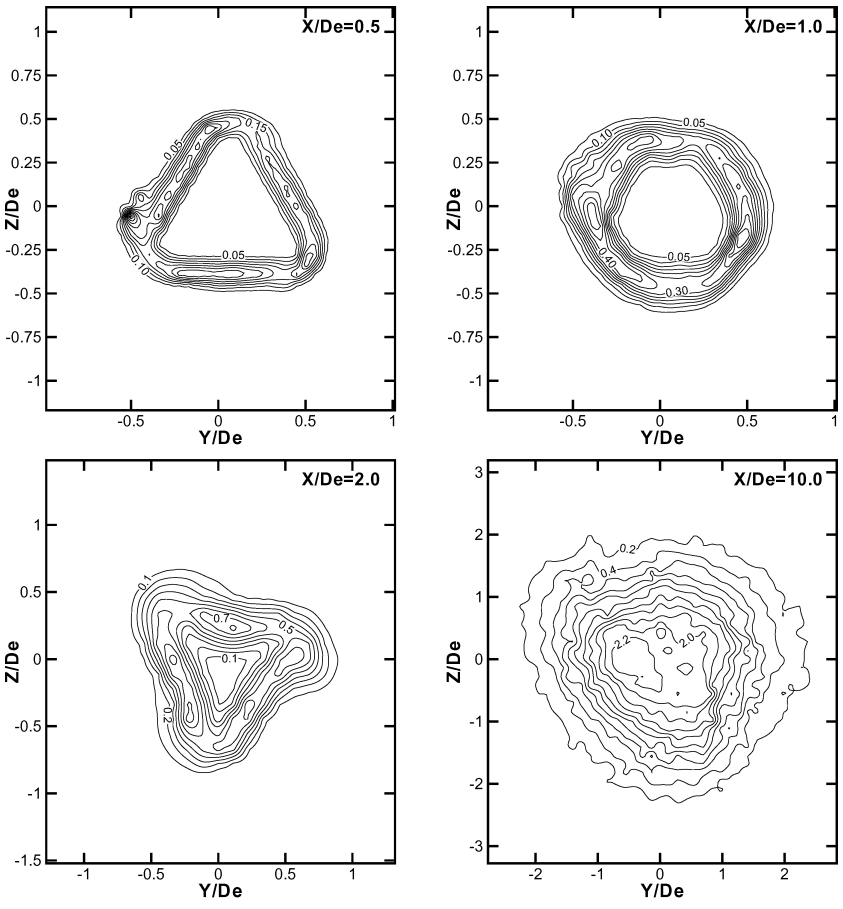

Fig. 14 Lateral Reynolds normal stress, $\overline{w'^2}/U_{cl}^2 \times 100$, contour maps.

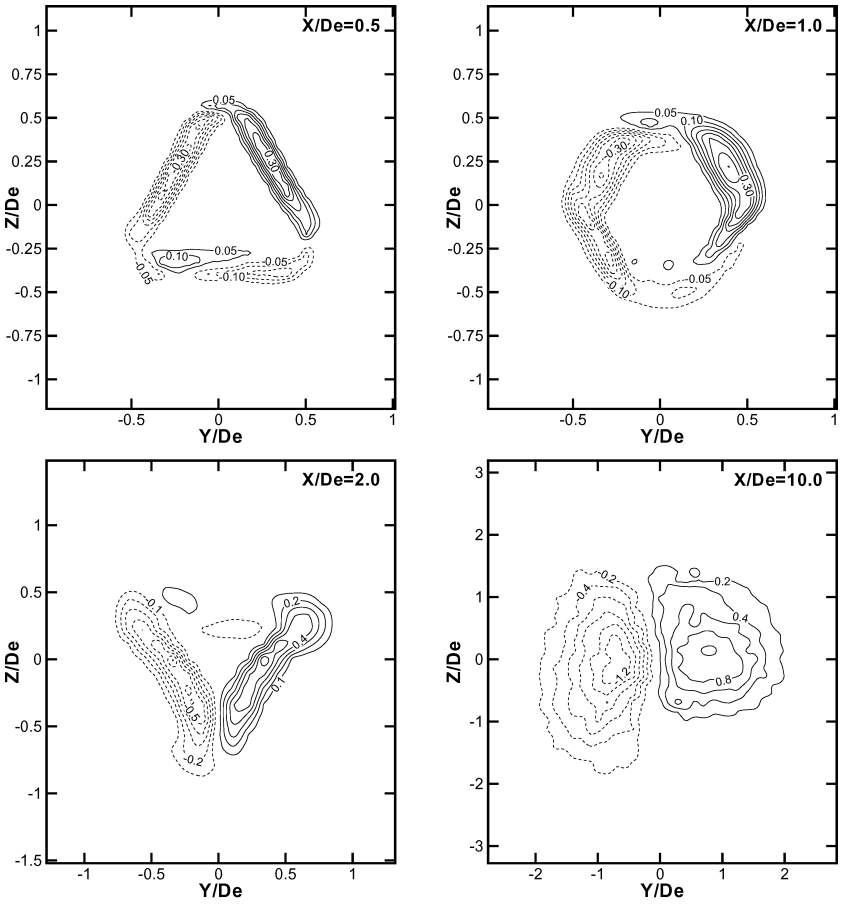

Fig. 15 Spanwise Reynolds primary shear stress, $\overline{u'v'}/U_{cl}^2 \times 100$, contour maps.

where the local shear in the mean streamwise velocity ($\partial U/\partial Y$, $\partial U/\partial Z$) is large or small. In the production of the streamwise Reynolds normal stress, for example, the major contributions are made by $-\overline{u'v'}\partial U/\partial Y$ and $-\overline{u'w'}\partial U/\partial Z$. This is why, as will become evident later, there is a close relationship between the streamwise Reynolds normal stress contour maps shown in Fig. 12 and the contour maps, which will be shown later, for the spanwise and lateral local shear in the mean streamwise velocity. The spanwise and lateral Reynolds normal stresses are generally smaller than the streamwise Reynolds normal stresses, from which they are obtained via the pressure fluctuations, at the corresponding locations in the flowfield. The estimated uncertainty in the measurement of the Reynolds normal stresses is $\pm 6\%$.

The spanwise Reynolds primary shear stress contour maps are shown in Fig. 15. The spanwise Reynolds primary shear stress represents the mean rate of transfer of the spanwise component of the linear momentum through a unit area normal to the streamwise direction. Contour maps for the local spanwise shear ($\partial U/\partial Y$) in the mean streamwise velocity are shown in Fig. 16 to facilitate the discussion of the spanwise Reynolds primary shear stress results. It is clear from Figs. 15 and 16 that the spanwise Reynolds primary shear stress is well correlated with the spanwise local shear in the mean streamwise velocity. This is not surprising because the dominant term in the generation of $\overline{u'v'}$ by the mean flow is $\overline{v'^2}\partial U/\partial Y$. This close correspondence between $\overline{u'v'}$ and $\partial U/\partial Y$ suggests that the stress–strain relationship $-\overline{u'v'} = \nu_t \partial U/\partial Y$ is valid in the current flow, implying that an isotropic turbulence model, such as the k–ε model, can be used to close the set of governing equations in the numerical computation of this flow.

The lateral Reynolds primary shear stress contour maps are shown in Fig. 17 and those for the local lateral shear ($\partial U/\partial Z$) in the mean streamwise velocity are shown in Fig. 18. The lateral Reynolds primary shear stress, which is produced from the mean flow mainly by the term $\overline{w'^2}\partial U/\partial Z$, is clearly well correlated with the strain ($\partial U/\partial Z$) as was the case with the spanwise Reynolds primary shear stress data discussed earlier. The estimated uncertainty in the measurement of the Reynolds primary shear stresses is $\pm 8\%$.

The distribution of the autocorrelation coefficients for the fluctuating streamwise velocity at various locations on the jet centerline in the near field of the jet is shown in Fig. 19. The autocorrelation coefficients of the fluctuating spanwise and lateral velocities were also measured but are not presented here for space reasons. The distribution of the autocorrelation coefficients is clearly periodic, indicating the presence of coherent structures, at $X/D_e = 0.5$, 1.0, and 2.0. In anticipation of the discussion of the one-dimensional energy spectra of the fluctuating streamwise velocity, note that the inverse of the time $t = 0.00155$ s, at which the distribution of the autocorrelation coefficients has its second maximum, is 645.16 Hz. The distribution of the autocorrelation coefficients at $X/D_e = 10.0$ represents that of a broadband signal, which is characteristic of fully turbulent flow.

The one-dimensional energy spectra of the fluctuating streamwise velocity on the jet centerline in the near flowfield are shown in Fig. 20. The one-dimensional energy spectra were obtained from fast Fourier transforms (FFT) of the digital hot-wire time-series data. At each location, the power spectra $\Phi(f)$ have been normalized by the square of the streamwise velocity fluctuation $\overline{u'^2}$. The one-dimensional energy spectra exhibit, consistent with the distribution of the autocorrelation coefficients shown in Fig. 19, discrete peaks at a frequency of 645.16 Hz at $X/D_e = 0.5$, 1.0, and 2.0. The magnitude of the spectral peaks reaches a maximum at $X/D_e = 2.0$. The spectral peaks indicate the passage of coherent structures. The one-dimensional energy spectrum of the fluctuating streamwise velocity at $X/D_e = 10.0$ is broadband, a characteristic of fully turbulent flow.

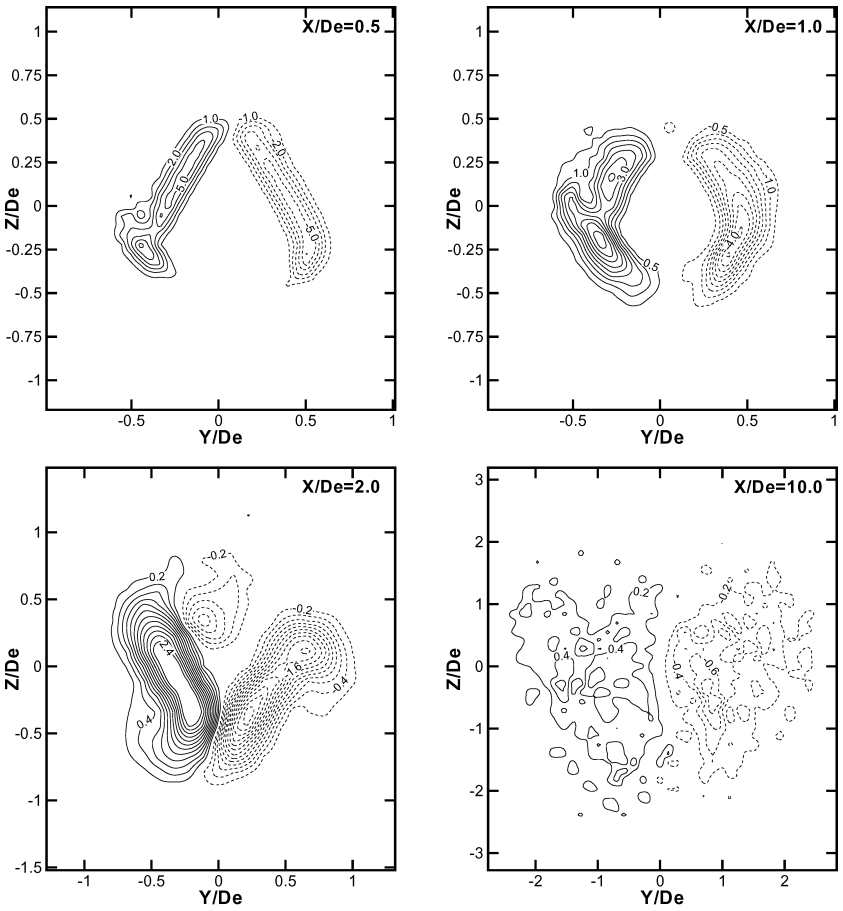

Fig. 16 Spanwise shear, $\partial U/\partial Y$, in mean streamwise velocity contour maps.

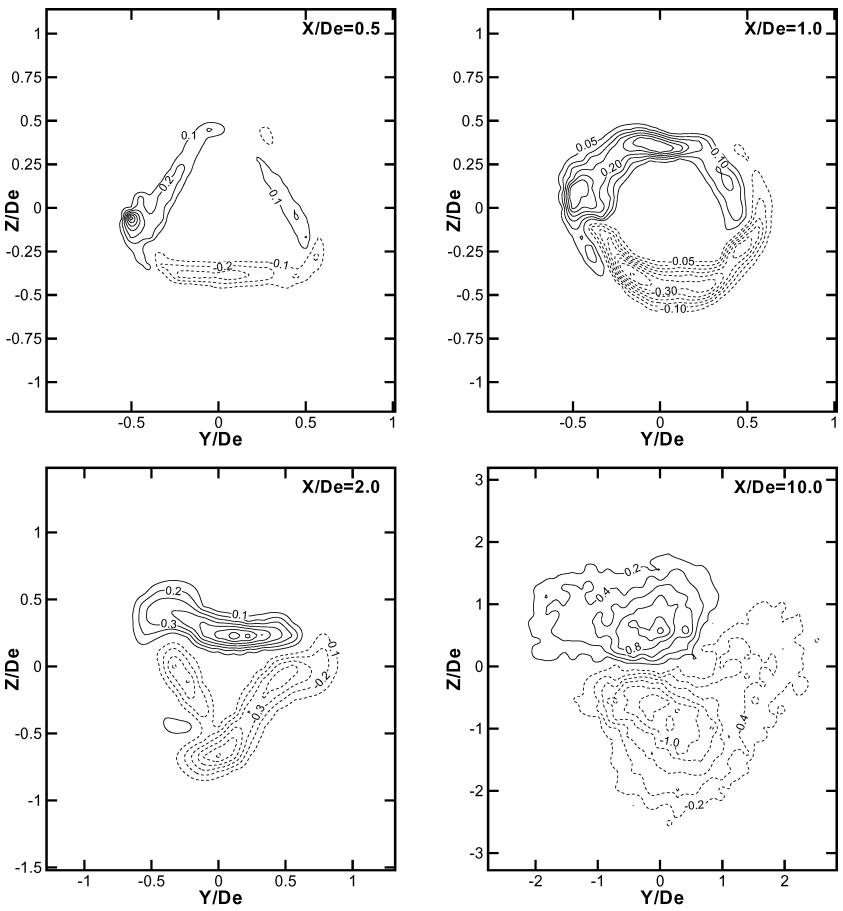

Fig. 17 Lateral Reynolds primary shear stress, $\overline{u'w'}/U_{cl}^2 \times 100$, contour maps.

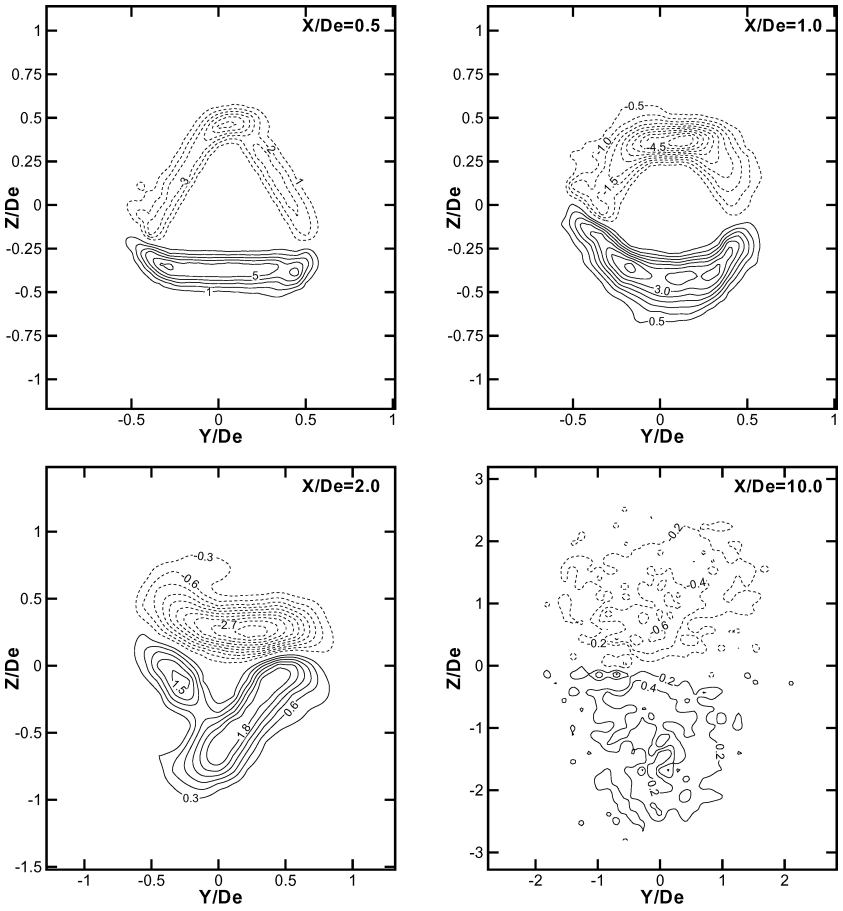

Fig. 18 Lateral shear, $\partial U/\partial Z$, in mean streamwise velocity contour maps.

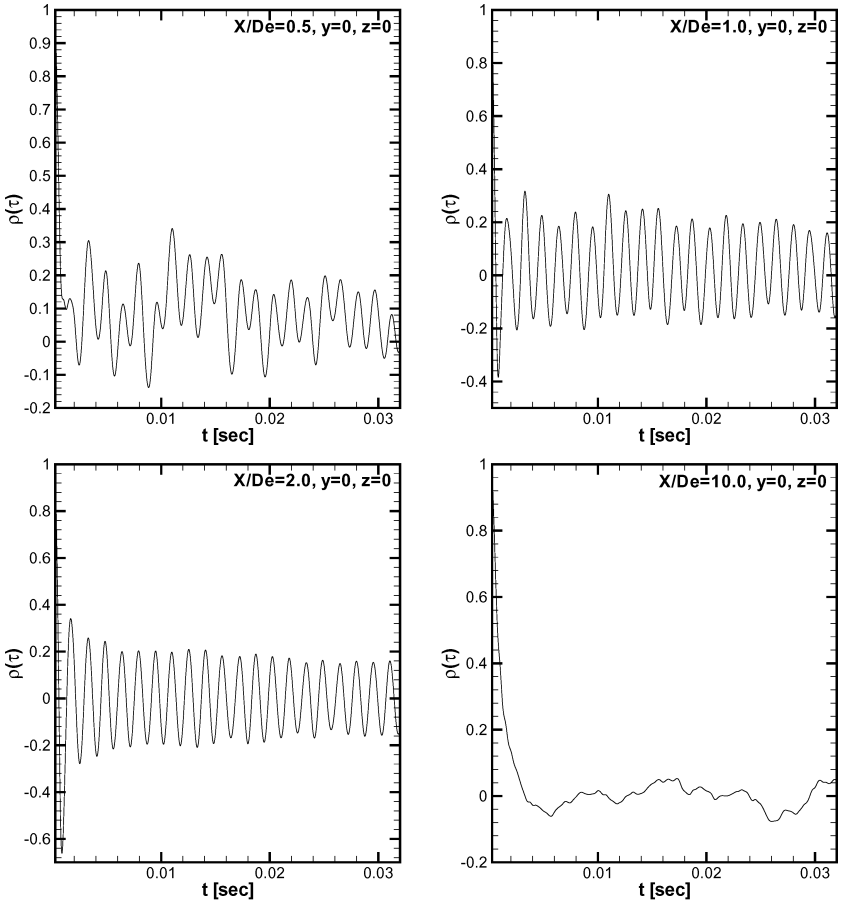

Fig. 19 Distribution of autocorrelation coefficients of the fluctuating streamwise velocity on jet centerline.

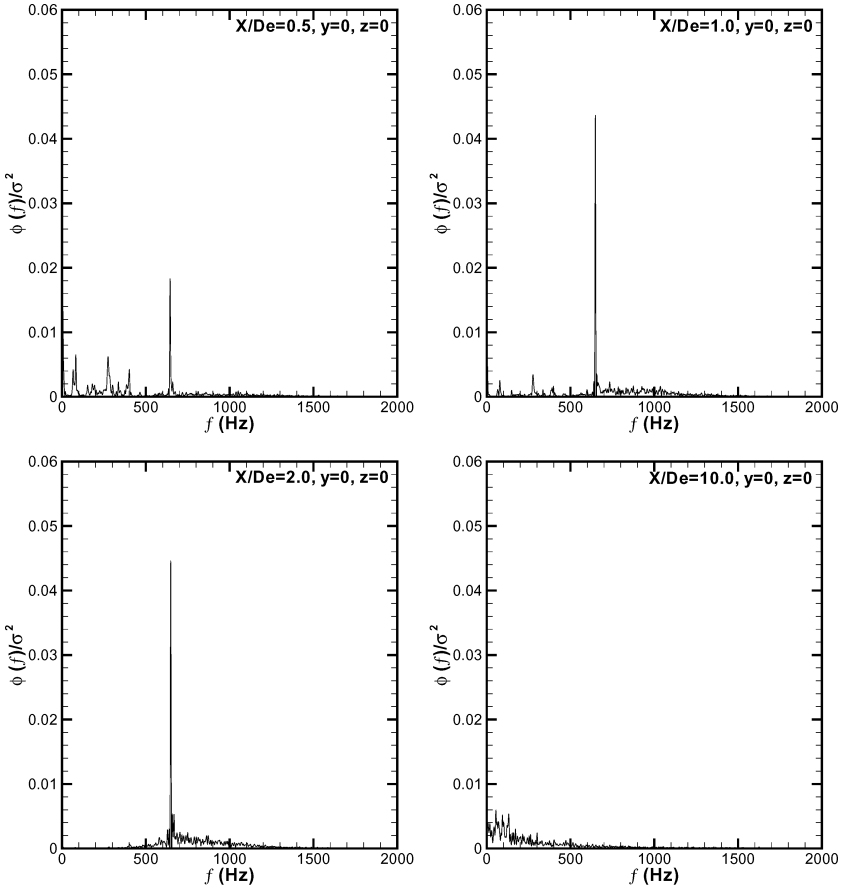

Fig. 20 One-dimensional energy spectra of fluctuating streamwise velocity on jet centerline.

Conclusions

The near flowfield of a turbulent freejet of air issuing from a sharp-edged equilateral triangular orifice into still air surroundings has been studied experimentally using hot-wire anemometry and a pitot-static tube. For the purpose of comparison, some measurements were made in a round jet that also issued from a sharp-edged orifice. The following conclusions are drawn from the results:

1) Mixing in the equilateral triangular jet is, as measured by the entrainment of ambient fluid, the spread of the jet, the peaking of the turbulence intensity on the jet centerline, and the recovery of the mean static pressure on the jet centerline, faster than in the round jet.

2) The mean streamwise vorticity field in an equilateral triangular jet is dominated by counter-rotating pairs of vortices aligned, initially, with the corners of the equilateral triangle. These vortices facilitate mixing and entrainment in the jet.

3) Large-scale coherent structures, which enhance mixing in the jet, are present in the near field of the equilateral triangular jet.

Acknowledgment

The ongoing financial support of the Natural Sciences and Engineering Research Council of Canada, through Operating Grant RGPIN 5484, is gratefully acknowledged.

References

[1]Gutmark, E. J., and Grinstein, F. F., "Flow Control with Noncircular Jets," *Annual Review of Fluid Mechanics*, Vol. 31, 1999, pp. 239–272.

[2]Vandsburger, U., and Ding, C., "The Spatial Modulation of a Forced Triangular Jet," *Experiments in Fluids*, Vol. 18, No. 4, 1995, pp. 239–248.

[3]Quinn, W. R., "Mean Flow and Turbulence Measurements in an Equilateral Triangular Turbulent Free Jet," *International Journal of Heat and Fluid Flow*, Vol. 11, No. 3, 1990, pp. 220–224.

[4]Schadow, K. C., Gutmark, E., Parr, D. M., and Wilson, K. J., "Selective Control of Flow Coherence in Triangular Jets," *Experiments in Fluids*, Vol. 6, No. 2, 1988, pp. 129–135.

[5]Gutmark, E., Schadow, K. C., Parr, T. P., Hanson-Parr, D. M., and Wilson, K. J., "Noncircular Jets in Combustion Systems," *Experiments in Fluids*, Vol. 7, No. 4, 1989, pp. 248–258.

[6]Miller, R. S., Madnia, C. K., and Givi, P., "Numerical Simulation of Non-Circular Jets," *Computers and Fluids*, Vol. 24, No. 1, 1995, pp. 1–25.

[7]Mi, J., Nathan, G. J., and Luxton, R. E., "Centerline Mixing Characteristics of Jets from Nine Differently Shaped Nozzles," *Experiments in Fluids*, Vol. 28, No. 1, 2000, pp. 93, 94.

[8]Bradshaw, P., *An Introduction to Turbulence and Its Measurement*, Pergamon, Oxford, 1974, pp. 121–123.

[9]Bearman, P. W., "Corrections for the Effect of Ambient Temperature Drift on Hot-Wire Measurements in Incompressible Flow," *DISA Information*, Vol. 11, May 1971, pp. 25–30.

[10]Bell, J. H., and Mehta, R. D., "Three-Dimensional Structure of Plane Mixing Layers," Joint Inst. of Aeronautics and Astronautics, Rept. TR-90, Dept. of Aeronautics and Astronautics, Stanford Univ., Stanford, CA, March 1989.

[11]Quinn, W. R., "Streamwise Evolution of a Square Jet Cross Section," *AIAA Journal*, Vol. 30, No. 12, 1992, pp. 2852–2857.

R. Lucht
Associate Editor